

An alternative approach to modelling a cosmic void and its effect on the cosmic microwave background

Do Young Kim,^{1,2★} Anthony N. Lasenby,^{1,2†} and Michael P. Hobson^{1‡}

¹*Astrophysics Group, Cavendish Laboratory, JJ Thomson Avenue, Cambridge CB3 0HE*

²*Kavli Institute for Cosmology, Madingley Road, Cambridge CB3 0HA*

Accepted XXX. Received YYY; in original form ZZZ

ABSTRACT

We apply our tetrad-based approach for constructing spherically-symmetric solutions in general relativity to modelling a void, and compare it with the standard Lemaître–Tolman–Bondi (LTB) formalism. In particular, we construct models for the void observed in the direction of Draco in the WISE-2MASS galaxy survey, and a corresponding cosmic microwave background (CMB) temperature decrement in the Planck data in the same direction. We find that the present-day density and velocity profiles of the void are not well constrained by the existing data, so that void models produced from the two approaches can differ substantially while remaining broadly consistent with the observations. We highlight the importance of considering the velocity as well as the density profile in constraining voids.

Key words: cosmology: theory – cosmic background radiation – large-scale structure of Universe

1 INTRODUCTION

It is of interest in cosmology to model non-linear structures such as clusters and voids, and determine the secondary temperature anisotropies that they induce in the cosmic microwave background (CMB). Recent attention has focussed in particular on voids, which arise naturally in Λ CDM cosmologies through the evolution of large scale structure, surrounded by filaments and clusters in the cosmic web (Colless et al. 2001; Tegmark et al. 2003; Sutter et al. 2012). Indeed, voids are of particular interest since their distribution is sensitive to the equation of state of dark energy (Pisani et al. 2015; Lavaux & Wandelt 2012). Moreover, the presence of our Galaxy within a large local void has been suggested as an alternative explanation for observations of the acceleration of the universal expansion, without invoking dark energy (Célérier 2012a,b; Bolejko & Célérier 2010; Bene & Csapo 2010; Kainulainen & Marra 2009; Marra et al. 2007b,a; Alexander et al. 2007) although it is likely that only a small part of the observed acceleration could be due to such an effect (Geshnizjani et al. 2005; Siegel & Fry 2005; Zibin et al. 2008).

Individual clusters and voids are often modelled as spherically-symmetric, pressureless systems using the

Lemaître–Tolman–Bondi (LTB) metric (Romano & Vallejo 2015; Tokutake & Yoo 2016; Finelli et al. 2016; Brouzakis et al. 2006). The LTB model is usually expressed in comoving coordinates and thus provides a Lagrangian picture of the fluid evolution. Such models can accommodate an arbitrary, usually continuous, density profile for the central object, but do have some limitations. For example, the central object is usually only compensated at infinity, which can complicate the interpretation of observational effects, since observers comoving with the cosmological fluid are not in a region modelled by a homogeneous Friedmann–Robertson–Walker (FRW) cosmology. In principle, compensation at a finite radius can be achieved by an appropriate choice of initial radial density and velocity profiles, but in so doing care must be taken to avoid subsequent streamline crossing, since the presence of shock fronts would necessitate the inclusion of pressure to produce a realistic model. Finally, the LTB metric contains a residual gauge freedom that necessitates the imposition of arbitrary initial conditions to determine the system evolution.

As a consequence, we have for some time adopted a different, tetrad-based method for solving the Einstein field equations for spherically-symmetric systems (Lasenby et al. 1998; Nandra et al. 2012a,b, 2013; Kim et al. 2018). Aside from straightforwardly accommodating pressure (which we will not consider here), the method has no gauge ambiguities in non-vacuum regions and is expressed in terms of a non-comoving radial coordinate that results in a Eulerian

★ dyk25@mrao.cam.ac.uk

† a.n.lasenby@mrao.cam.ac.uk

‡ mph@mrao.cam.ac.uk

picture of the fluid evolution with a clear physical interpretation. Indeed, the gauge choices employed lead to dynamical equations that are essentially Newtonian in form. Assuming a pressureless fluid throughout, we have already applied the method to modelling the evolution of a finite-size, spherically-symmetric cluster, with continuous radial density and velocity profiles, that is embedded in an expanding background universe and compensated so that it does not exert any gravitational influence on the exterior universe (Lasenby et al. 1999; Dabrowski et al. 1998, 1999). In our approach, one considers an initial velocity profile from which the initial density profile is determined uniquely by the constraints that there are no decaying modes present and that the density distribution is compensated. Moreover, this compensation holds at all later times, and the velocity field evolves in a way that avoids streamline crossing.

In this paper, we apply our approach to modelling voids and calculate their effect on the CMB. As a particular example, we consider the Draco supervoid, for which the present day density and velocity profiles have been estimated by Finelli et al. (2016) (hereinafter FGKPS) from a projected underdensity in the WISE-2MASS galaxy survey and a CMB temperature decrement in the Planck data in the same direction. We consider a number of ways in which a similar void can be produced in our approach, and determine the resulting temperature decrements, with particular focus on the influence of the void velocity profile. We also compare our results with those derived previously using the LTB model.

The structure of this paper is as follows. In Section 2, we introduce the tetrad-based method, and the model we use for spherical perturbations that are consistent with having evolved from primordial fluctuations in the early universe. In Section 3, we discuss the LTB void model used by Finelli et al. (2016); Mackenzie et al. (2017); Marcos-Caballero et al. (2016); Zibin (2014); Nadathur et al. (2014) in their analyses of supervoids. We then compare CMB decrements caused by voids similar to the LTB model used to represent the Draco supervoid by FGKPS in Sections 5 and 6. Lastly we present our conclusions in Section 7.

2 TETRAD-BASED METHODOLOGY AND VOID MODEL

Our tetrad-based approach is summarised in Kim et al. (2018). In a Riemannian spacetime, the relationship between the coordinate basis vectors \mathbf{e}_μ and local Lorentz frame vectors $\hat{\mathbf{e}}_a$ are given by the tetrads, or vierbeins e_a^μ , where the inverse is denoted e^a_μ , such that $\hat{\mathbf{e}}_a = e_a^\mu \mathbf{e}_\mu$ and $\mathbf{e}_\mu = e^a_\mu \hat{\mathbf{e}}_a$. Assuming spherical symmetry and a pressureless fluid, one may adopt a gauge in which the non-zero tetrad components are given by $e_0^0 = 1$, $e_0^1 = g_2$, $e_1^1 = g_1$, $e_2^2 = 1/r$ and $e_3^3 = 1/(r \sin \theta)$, where $g_1(r, t)$ and $g_2(r, t)$ are unknown functions. Note that dependencies on both r and t will often be suppressed in the equations presented below, whereas we will usually make explicit dependency on either r or t alone. The gauge adopted is called the Newtonian gauge (not to be confused with that used in perturbation theory) because it allows simple Newtonian interpretations of the dynamics. In this gauge, the metric coefficients derived from the tetrad

components lead to the line-element

$$ds^2 = \left(1 - \frac{g_2^2}{g_1^2}\right) dt^2 + \frac{2g_2}{g_1^2} dt dr - \frac{1}{g_1^2} dr^2 - r^2 d\Omega^2. \quad (1)$$

The time coordinate t measures the proper time of observers comoving with the fluid, and the (non-comoving) radial coordinate r labels spheres of proper area $4\pi r^2$. It is straightforward to show that g_2 is the rate of change of the r coordinate of a fluid particle (or comoving observer) with respect to its proper time, and so can be physically interpreted as the fluid 3-velocity. As demonstrated below, the physical interpretation of g_1 is such that the total energy per unit mass of a fluid particle is $\frac{1}{2}(g_1^2 - 1)$ (after subtraction of the rest-mass energy).

2.1 Field equations

For a fluid with density $\rho(r, t)$, the total mass-energy, $M(r, t)$, contained in a sphere of radius r is given by

$$\frac{\partial M}{\partial r} = 4\pi r^2 \rho, \quad (2)$$

and the mass flow through a sphere of radius r per unit time is given by

$$\frac{\partial M}{\partial t} = -4\pi r^2 \rho g_2. \quad (3)$$

As mentioned above, the variable g_2 may be interpreted physically as the fluid 3-velocity in the coordinate frame and defines the integral curves of the conserved fluid current by

$$\frac{dr}{dt} = g_2. \quad (4)$$

These integral curves are also matter geodesics, since the fluid is pressureless. For functions of both r and t , one can therefore define the comoving derivative

$$\frac{d}{dt} = \frac{\partial}{\partial t} + g_2 \frac{\partial}{\partial r}, \quad (5)$$

which determines the rate of change of a quantity along a streamline with respect to the proper time of a comoving fluid element. From equations (2) and (3), one thus sees that M is conserved along a streamline, such that

$$\frac{dM}{dt} = 0, \quad (6)$$

which prohibits the possibility of streamline crossing.

The continuity equation has the form

$$\frac{d\rho}{dt} = -\left(\frac{2g_2}{r} + H\right)\rho, \quad (7)$$

where we have defined the velocity gradient

$$H(r, t) \equiv \frac{\partial g_2}{\partial r}. \quad (8)$$

Euler's equation is given by

$$\frac{dg_2}{dt} = -\frac{M}{r^2} + \frac{1}{3}\Lambda r, \quad (9)$$

the integral of which along a streamline gives the Bernoulli equation,

$$\frac{1}{2}g_2^2 - \left(\frac{M}{r} + \frac{1}{6}\Lambda r^2\right) = \frac{1}{2}(g_1^2 - 1). \quad (10)$$

This provides the physical interpretation of g_1 discussed above. Indeed, by applying the comoving derivative (5) to (10), and using (9), one finds the useful result,

$$\frac{dg_1}{dt} = 0, \quad (11)$$

which demonstrates that g_1 is conserved along a streamline.

It is most natural to specify the initial data for the above set of equations in terms of the density and 3-velocity profiles, $\rho(r, t_i)$ and $g_2(r, t_i)$, at some initial time t_i . From these one can calculate $M(r, t_i)$ and $g_1(r, t_i)$, which are then conserved along the streamlines.

2.2 Streamline equations

The equations (4) and (10) can be solved analytically using elliptic integrals to obtain the position r at some time t of a fluid particle, given its position r_i at some initial time t_i . It is often simpler, however, instead to solve numerically the system of first-order ordinary differential equations (4) and (9), namely (Dabrowski et al. 1999):

$$\frac{dr}{dt} = g_2, \quad (12)$$

$$\frac{dg_2}{dt} = -\frac{M(r_i)}{r^2} + \frac{\Lambda}{3}r, \quad (13)$$

where r_i is the position of the fluid particle on some streamline at an initial time t_i . These equations can be integrated simultaneously to find the position and velocity of the given fluid particle at a later time t , using the fact that $M(r_i)$ is constant on a given streamline. The fluid density $\rho(r, t)$ and velocity gradient $H(r, t)$ are obtained by performing the numerical differentiation in equations (2) and (8). Hence, given some initial conditions for the density and velocity distributions, $\rho(r, t_i)$ and $g_2(r, t_i)$, the entire system is determined.

2.3 Initial conditions

We demand that the void has grown from primordial fluctuations in the early universe. At such early epochs, it is valid to linearise the field equations around a homogeneous cosmology, which yields two solutions: a growing mode and a decaying mode. By demanding that the decaying mode is absent, and assuming a flat- Λ background cosmology, one finds that the initial velocity and mass distributions are related by (Dabrowski et al. 1999)

$$g_2(t_i, r) = \frac{2r}{3H_i} \left(2H_i^2 - \frac{M_i}{r^3} - \frac{\Lambda}{6} \right). \quad (14)$$

This is equivalent to imposing the following relationship between the initial velocity and density distributions

$$\rho(t_i, r) = \frac{3H_i}{8\pi} \left(4H_i - \frac{2g_{2,i}}{r} - H - \frac{\Lambda}{3H_i} \right). \quad (15)$$

2.4 Photon equations

The photon trajectory can be parameterised using t , such that it is defined by $r(t)$ and $\phi(t)$, where $\phi(t)$ is the azimuthal angle in spherical coordinates. Without loss of generality, we may assume that the trajectory lies in the $\theta = \pi/2$ plane.

The requirement that the trajectory is null leads to the conditions

$$\begin{aligned} \frac{dr}{dt} &= g_1 \cos \chi + g_2, \\ \frac{d\phi}{dt} &= \frac{\sin \chi}{r}, \end{aligned} \quad (16)$$

where χ is the angle, as measured by observers comoving with the fluid, between the photon path and centre of the void (which we set to lie at the origin $r = 0$). The geodesic equations then determine how χ evolves with time:

$$\frac{d\chi}{dt} = \sin \chi \left[\cos \chi \left(H - \frac{g_2}{r} \right) - \frac{g_1}{r} \right]. \quad (17)$$

These equations are sufficient to calculate the position of the photon along its trajectory, and are easier to integrate numerically than the usual second-order geodesic equations. The trajectory is determined by an initial set of data r_i , ϕ_i and χ_i . For most calculations, however, the data are provided in the form of the observer's position and an angle on the sky χ , and the equations are then run backwards in time to take the photon back through the void.

The remaining content of the geodesic equations determines the evolution of the photon frequency ω , as measured by a comoving observer:

$$\frac{d\omega}{dt} = -\omega \left(H \cos^2 \chi + \frac{g_2}{r} \sin^2 \chi \right). \quad (18)$$

One can show from the above equations that the angular momentum of the photon, $L = -r^2 \omega d\phi/dt = -\omega r \sin \chi$, is conserved.

To calculate the effect of the void on a CMB photon, we first write

$$g_2(t, r) = rH_e(t) + \Delta(t, r), \quad (19)$$

where $H_e(t)$ is the Hubble function in the exterior Universe at time t , and Δ is thus the difference between the equivalent fluid velocity in the unperturbed Universe and in the void. One may then show that the physically measurable CMB temperature decrement due to the void is given by (Lasenby et al. 1999)

$$\frac{\Delta T}{T} = e^{-\epsilon} - 1 \approx -\epsilon, \quad (20)$$

where the small quantity ϵ is defined by

$$\epsilon = \int_{t_1}^{t_2} dt \left(\frac{\partial \Delta}{\partial r} \cos^2 \chi + \frac{\Delta}{r} \sin^2 \chi \right). \quad (21)$$

This integral is evaluated along the photon path between the time the photon enters the void (t_1) and the time it leaves (t_2). The function ϵ is small, since the contribution to the integral from near the void centre tends to cancel the contributions from further out. The main effect producing a non-zero ϵ is essentially the evolution of Δ with time.

2.5 Void model

Our void model is based on that used to model a cluster in Dabrowski et al. (1998). The nature of the void is determined by specifying the velocity distribution $g_2(r, t_i)$ at some initial time t_i in terms of four parameters H_i , R_i , a and m . Here, $H_i \equiv H_e(t_i)$ is the background Hubble parameter at $t = t_i$, R_i is the initial size of the perturbed region, and

a is the velocity gradient at the origin (which determines the magnitude of the perturbation). For $r < R_i$, the fluid velocity is described by a polynomial in r of order $2m + 1$, and the first m radial derivatives are matched at the boundaries, $r = 0$ and $r = R_i$. For $r > R_i$, the fluid velocity is that of the background $g_2(r, t_i) = rH_i$. The initial density profile $\rho(r, t_i)$ is then determined using equation (15), such that the density is a polynomial of order $2m$. One can show that the resulting initial density profile is compensated, and hence remains compensated for all time. Consequently, in the external region ($r > R_i$) the fluid evolves as a homogeneous FRW universe. Placing observers in this region allows for unambiguous calculations of the CMB perturbation caused by the void. Once the initial velocity and density profiles are defined, the evolution of the fluid is then completely determined.

A velocity gradient at the origin that is slightly greater than that of the unperturbed universe, so that $a > H_i$, leads to the formation of a void (and, conversely, setting $a < H_i$ would lead to the formation of a cluster). Also, the boundary conditions imply that when the value of m is greater than unity, the density gradient is zero at the origin, whereas this condition is not necessarily satisfied for $m = 1$; hence we choose $m \geq 2$ for a sensible density profile.

3 LTB MODEL

Having discussed our own methodology for modelling voids, we now turn to an approach based on the LTB model, and establish the relations between quantities in the two models.

The LTB metric (Lemaître 1933; Tolman 1934; Bondi 1947) describes a spherically-symmetric pressureless system, and may be written in the form

$$ds^2 = d\hat{t}^2 - \frac{(\partial_{\hat{r}} R)^2}{1 + 2E(\hat{r})} - R^2 d\Omega^2, \quad (22)$$

where \hat{r} is a comoving radial coordinate and the time coordinate \hat{t} coincides with the proper time measured by observers comoving with the fluid. The function R depends, in general, on both \hat{t} and \hat{r} , and the function $E(\hat{r})$ determines the so-called ‘curvature profile’ of the system, and may be specified arbitrarily, provided $E(\hat{r}) > -\frac{1}{2}$.

As discussed in Kim et al. (2018), one may transform the line-element (1) used in our tetrad-based approach into the LTB line-element (22) via the coordinate transformation

$$t = \hat{t}, \quad r = R(\hat{r}, \hat{t}), \quad \text{where} \quad \frac{\partial R}{\partial \hat{t}} = g_2, \quad (23)$$

and in so doing one makes the further identification $g_1^2 = 1 + 2E(\hat{r})$, which confirms the usual alternative interpretation of $E(\hat{r})$ as the energy per unit mass of a fluid particle (after subtracting its rest mass). One may also show that partial derivatives in the two coordinate systems are related by

$$\frac{\partial}{\partial \hat{t}} = \frac{\partial}{\partial t} + g_2 \frac{\partial}{\partial r} = \frac{d}{dt}, \quad (24)$$

$$\frac{\partial}{\partial \hat{r}} = \frac{\partial R}{\partial \hat{r}} \frac{\partial}{\partial r}. \quad (25)$$

Since $\frac{d}{dt}$ is the convective derivative, the transformation (23) is naturally interpreted as moving from a Eulerian to a Lagrangian description of the fluid motion.

In LTB coordinates, one finds $\partial_{\hat{t}} M = 0$, so that $M = M(\hat{r})$, which is interpreted as the mass contained within the comoving radius \hat{r} . The remaining Einstein equations become

$$\partial_{\hat{r}} M(\hat{r}) = 4\pi R^2 \rho \partial_{\hat{r}} R, \quad (26)$$

$$(\partial_{\hat{r}} R)^2 = 2E(\hat{r}) + \frac{2M(\hat{r})}{R} + \frac{1}{3}\Lambda R^2. \quad (27)$$

The latter is the LTB equivalent of the Bernoulli equation (10), for which the solution $R(\hat{r}, \hat{t})$ can be written in integral form as

$$\hat{t} - \hat{t}_B(\hat{r}) = \int_0^{R(\hat{r}, \hat{t})} \frac{dA}{\sqrt{2E(\hat{r}) + \frac{2M(\hat{r})}{A} + \frac{1}{3}\Lambda A^2}}, \quad (28)$$

where the function $\hat{t}_B(\hat{r})$ is known as the bang-time, which is interpreted as a Big-Bang singularity surface at which R vanishes, i.e. $R(\hat{r}, \hat{t}_B(\hat{r})) = 0$, and may be chosen arbitrarily.

In the LTB model, one is thus required to specify three arbitrary time-independent functions. The functions $E(\hat{r})$ and $\hat{t}_B(\hat{r})$ are usually interpreted as determining the nature of the system, and the remaining gauge freedom in redefining the radial coordinate is usually removed by specifying $M(\hat{r})$. In this case, (28) can then be solved for $R(\hat{r}, \hat{t})$, so that metric (22) is fully determined, and the corresponding density $\rho(\hat{r}, \hat{t})$ is found from (26). A common alternative gauge-fixing procedure is instead to specify $R(\hat{r}, \hat{t}_0)$, where \hat{t}_0 denotes the current epoch \hat{t}_0 . In this case, (28) is then solved at \hat{t}_0 for $M(\hat{r})$, before proceeding as before. It is worth noting that, in order for no decaying mode to be present, one requires $\hat{t}_B(\hat{r})$ not to be spatially varying, and one may choose $\hat{t}_B = 0$ without loss of generality (Zibin 2008).

4 MODELLING THE DRACO VOID

We now wish to compare our tetrad-based approach with the LTB model in the context of modelling a specific void structure. Our main aim will be to show that in comparing void models with CMB data, both the underlying density and velocity profiles of the void are important, and should both be considered. We also wish to demonstrate, however, that the tetrad-based approach is simpler and more intuitive in some respects than the LTB model, although the latter does of course remain a valid approach. Indeed, when the issues related to density versus velocity profile are set aside, the quantitative differences that arise between the two methods in modelling the cosmic void considered below are only at the few per cent level.

The particular approach we consider is that adopted by Finelli et al. (2016) (hereinafter FGKPS). They used the LTB metric to model compensated voids and showed that a large void can lead to a significant temperature decrement in the CMB. Indeed, in the first version of their paper (Finelli et al. 2014), and following their identification of a projected underdensity in the WISE-2MASS all-sky infrared galaxy catalogue aligned with the CMB Cold Spot direction, they originally stated that a supervoid of size ~ 400 Mpc and depth (fractional overdensity) $\delta \sim -0.10$ can explain the Cold Spot temperature decrement of $\Delta T \sim 150 \mu\text{K}$; they also stated that this decrement is mostly due to the Rees–Sciama (RS) effect (Finelli et al. 2014), rather than the linear integrated Sachs–Wolfe (ISW) effect. Nonetheless, it was later

shown by Zibin (2014) and Nadathur et al. (2014), again using the LTB approach, that the ISW effect dominates and that a void of these proportions is not capable of producing such a large CMB decrement. In the later version of their paper, FGKPS accept that the Cold Spot decrement is difficult to explain by the presence of a single supervoid only, but drew attention to another sky area where a large under-density in the projected WISE-2MASS galaxy map (which they call the Draco supervoid) can account for the CMB decrement observed in that direction.

In this section, we therefore summarise the LTB approach used by FGKPS to describe the Draco supervoid and then in the following section compare the results of this model with what is obtained using our own tetrad-based model.

4.1 Modelling the Draco void using an LTB approach

To model the Draco void, FGKPS choose the curvature profile to have the form

$$E(\hat{r}) = E_0 \hat{r}^2 \exp\left(-\frac{\hat{r}^2}{\hat{r}_0^2}\right). \quad (29)$$

FGKPS do not specify their choice for the bang-time $\hat{t}_B(\hat{r})$, but we presume that it is set to a constant (which one may take to be zero) so that their model contains no decaying mode. FGKPS also do not specify their gauge choice, but reference is made to an earlier work (Garcia-Bellido & Haugbølle 2008) in which they fix the gauge by setting $R(\hat{r}, \hat{t}_0) = \hat{r}$. From (26), this is equivalent to setting $M(\hat{r}) = \frac{4\pi}{3} \hat{r}^3 \rho(\hat{r}, \hat{t}_0)$, where $M(\hat{r})$ is determined from (28).

FGKPS also appear to fix the present-day density contrast, which as pointed out by Nadathur et al. (2014) could over-constrain their model, and we discuss this aspect further below. In particular, they assume the curvature profile (29) to correspond to a perturbation Φ in the synchronous gauge in a spatially-flat Λ CDM model. Treating the perturbation as linear gives rise to the present-day metric perturbation $\Phi(\hat{r}) = \Phi_0 \exp(-\hat{r}^2/\hat{r}_0^2)$. Taking the growing mode and using the Poisson equation, FGKPS obtain the present-day density contrast

$$\delta(\hat{r}) = -\delta_0 \left(1 - \frac{2\hat{r}^2}{3\hat{r}_0^2}\right) \exp\left(-\frac{\hat{r}^2}{\hat{r}_0^2}\right), \quad (30)$$

which is plotted in Fig. 1 and ensures that the void is compensated at infinity.

This density contrast (projected onto the sky) and the CMB decrement produced by the RS and ISW effects calculated from the metric perturbation Φ are then used in a simultaneous χ^2 fit to the void in the WISE-2MASS galaxy catalogue and Planck CMB data to estimate the three parameters, δ_0 , r_0 and z_0 , where z_0 is defined as the redshift at the centre of the void. The best-fit values and 68 per cent confidence limits were found to be

$$\begin{aligned} \delta_0 &= 0.37^{+0.22}_{-0.12}, \\ r_0 &= 190^{+39}_{-27} \text{ Mpc}/h, \\ z_0 &= 0.15^{+0.04}_{-0.05}, \end{aligned} \quad (31)$$

where h is defined such that the current Hubble parameter is given by $H_0 = 100h \text{ km s}^{-1} \text{ Mpc}^{-1}$.

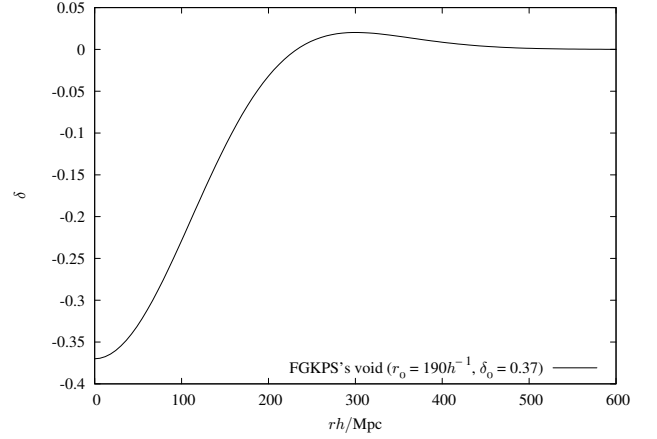


Figure 1. Present-day density contrast used by Finelli et al. (2016) to model the Draco supervoid.

4.2 Presence of decaying mode

If FGKPS do indeed specify both the gauge condition $R(\hat{r}, \hat{t}_0) = \hat{r}$ and the present-day density contrast (30), then it will not be possible, in general, to satisfy the constraint (28) with $\hat{t}_B(\hat{r})$ being equal to a constant (usually zero). Consequently, the void model would contain some contribution from a decaying mode, and thus be incompatible with the standard picture of cosmological structure formation (Zibin 2008; Nadathur et al. 2014).

To demonstrate this possibility, we calculate the quantity

$$\hat{t}'(\hat{r}) = \int_0^{\hat{r}} \frac{dA}{\sqrt{2E(\hat{r}) + \frac{2M(\hat{r})}{A} + \frac{1}{3}\Lambda A^2}}, \quad (32)$$

in which $E(\hat{r})$ is given by (29) and

$$M(\hat{r}) = \frac{4\pi\hat{r}^3}{3} \bar{\rho}(\hat{t}_0) (1 + \delta(\hat{r})), \quad (33)$$

where $\bar{\rho}(\hat{t}_0)$ is the present-day background FRW density and the present-day density contrast $\delta(\hat{r})$ is given by (30). If this specification were consistent with the absence of a decaying mode contribution, then $\hat{t}'(\hat{r})$ should be constant and equal to \hat{t}_0 , which is 13.5 Gyr for the assumed background cosmology.

In addition, FGKPS do not specify the value of E_0 used to set the amplitude of their curvature profile in (29). We therefore try two different methods to determine the value of E_0 . The first is to find the value of E_0 which minimises the rms variation of $\hat{t}'(\hat{r})$ over the range $0 < \hat{r} < 600$ Mpc. Using the best-fit values of δ_0 and \hat{r}_0 for the Draco supervoid given in (31), we find that the rms variation is minimised when $E_0 \hat{r}_0^2 = 5.3 \times 10^{-4}$. The second method is to treat the perturbation as having linearly grown (as outlined in Zibin (2014)). This results in $E_0 \hat{r}_0^2 = 4.78 \times 10^{-4}$. One would expect the nonlinear growth to deviate from this however, as the density contrast is fairly large.

The corresponding ratio $\hat{t}'(\hat{r})/\hat{t}_0$ is plotted in Fig. 2 for each value of E_0 , and clearly neither is constant and equal to unity. Indeed, $\hat{t}'(\hat{r})$ exhibits a ~ 2 per cent variation about a mean value of ≈ 13.2 Gyr. We may thus conclude that

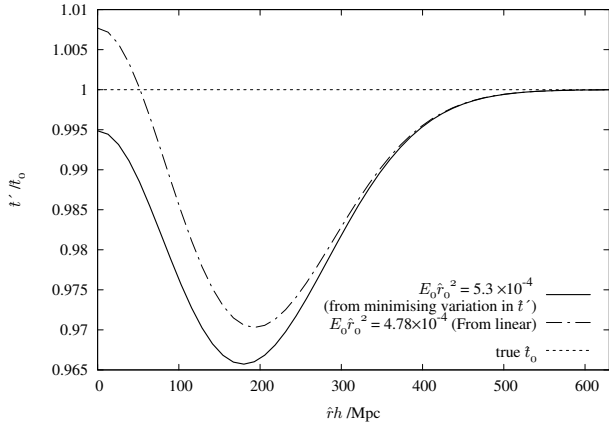


Figure 2. Plot of i' using different values of E_0 , using parameters for the Draco supervoid (31). The variation is at its smallest when $E_0 i_0^2 = 5.3 \times 10^{-4}$. As $\hat{r} \rightarrow \infty$, $i' \rightarrow i_0$ for all values of E_0 , as expected.

the resulting LTB model must have some contribution from a decaying mode, although the difference between the imposed present-day density profile and one that contains no decaying mode contribution is only at the level of a few per cent. This is in agreement with level of inconsistency found by Nadathur et al. (2014), who instead estimated the value of E_0 in the FGKPS model by minimising the difference $i'(\hat{r}) - i_0$ at the single point $\hat{r} = 0$ (Nadathur, private communication). Our findings are also consistent with those of Zibin (2014), who finds that the present-day density profile imposed by FGKPS differs from that obtained from (26) in a self-consistent LTB model, although again the discrepancy is small. In the rest of the paper we choose the value of E_0 found by minimising the rms variation in $i'(\hat{r})$, namely $E_0 i_0^2 = 5.3 \times 10^{-4}$.

5 REPRODUCING THE DRACO VOID

The issues outlined in the previous section arise, in part, from the subtleties associated with gauge-fixing in the LTB model, for which the physical interpretation is unintuitive. In this Section, we therefore instead model the Draco void using the tetrad-based approach described in Section 2, for which we believe the physical interpretation is clearer. Rather than simply fitting our model directly to the WISE-2MASS galaxy survey data and Planck CMB observations, however, we wish to focus on the different nature of the void characteristics in the LTB and tetrad-based approaches. Consequently, we will compare our model instead with the LTB model derived by FGKPS for the Draco void. In particular, we wish to determine the CMB temperature decrement produced by a void with present-day characteristics similar to those of the FGKPS void model for Draco, but modelled using our approach.

As mentioned in Section 2.5, in our approach the nature of the present-day void is determined by specifying the velocity distribution $g_2(r, t_i)$ at some initial time in terms of the four parameters H_i , R_i , a and m . We choose here to set these conditions at $z = 10^3$, since the perturbations are

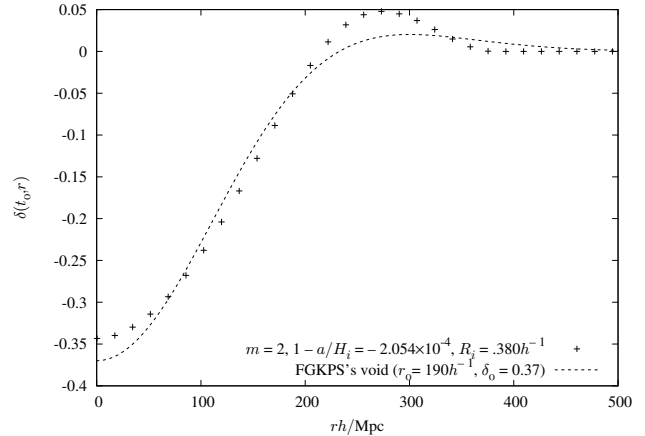


Figure 3. Void density profile at $t = t_0$ in our model (crosses), resulting from an initial velocity perturbation at $z = 10^3$ with parameters chosen to reproduce the FGKPS void density profile (solid line) as closely as possible.

safely within the linear regime at this epoch. The initial density distribution is then determined by the requirement that the decaying mode is absent in the linearised limit, as discussed in Section 2.3. Following FGKPS, we assume a spatially-flat Λ CDM background cosmology with $\Omega_\Lambda = 0.7$, for which $H_i = 1.735 \times 10^6 h \text{ km s}^{-1} \text{ Mpc}^{-1}$. To determine the appropriate values for the remaining parameters R_i , a and m , one has the choice of attempting to reproduce the present-day distribution in the FGKPS Draco void model of either: density, velocity, or both. We consider each of these in turn. As we will see, these options lead to very different CMB temperature decrements.

5.1 Reproducing the density profile

We begin by choosing the initial velocity perturbation parameters R_i , a and m such that the resulting present-day density profile of the void $\rho(r, t_0)$ is as similar as possible to that of the FGKPS Draco void model, which is plotted in Fig. 1.

This is achieved by performing a numerical optimisation in which the values of R_i , a and m are varied. For each set of parameter values, the resulting present-day density profile is evaluated at 40 equally-spaced points in the range $0 < r < 500 \text{ Mpc}$ and compared with the corresponding values in the FGKPS Draco void density profile. The optimal values of the parameters are those that minimise and sum of the squares of the differences in the two profiles. The resulting optimal present-day density profile is compared with the FGKPS density profile in Fig. 3. Given the very different underlying physical models, there is reasonably close agreement between the density profiles. In particular, we find that lower values of the parameter m are preferred, since they result in a smoother density profile in our model; we thus use $m = 2$ for the remainder of this section.

Since our primary interest, however, is in the CMB temperature decrement produced by our void, it is worth recalling from Section 2.4 that the main contribution to this effect is the evolution of the difference Δ between the equivalent

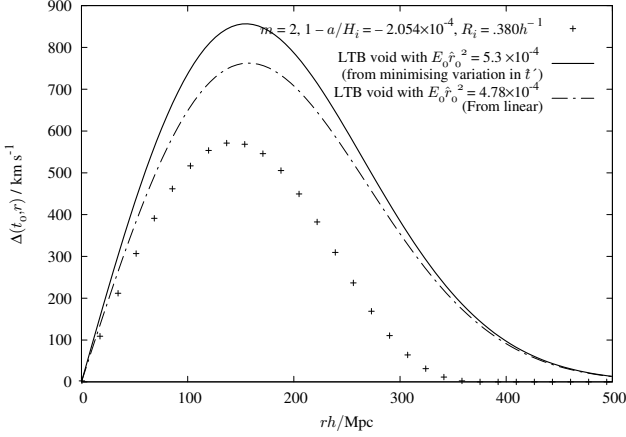


Figure 4. Difference $\Delta \equiv g_2 - rH_e$ at $t = t_0$ between the fluid velocity in the void and in the external universe for our void model (crosses) and the LTB void model of FGKPS for two different values of E_0 (solid and dotted lines).

fluid velocity in the external universe and in the void, as the CMB photon traverses it. Consequently, it is of interest also to compare the velocity distribution of our void to that of the FGKPS void.

To determine the velocity distribution of the FGKPS void, we note from (23) that the LHS of (27) gives the square of the fluid velocity in the LTB model at any given epoch. Using the forms for $E(\hat{r})$ and $M(\hat{r})$ given in (29) and (33), respectively, and employing the gauge condition $R(\hat{r}, \hat{t}_0) = \hat{r}$, one thus obtains the velocity profile at the current epoch. The corresponding Δ profile is plotted Fig. 4 for two different values of the parameter E_0 that defines the amplitude of the LTB curvature profile (solid and dotted lines), together with the Δ profile from our void (crosses). The solid line corresponds to the value of E_0 determined in Section 4.2, whereas the dotted lines corresponds to a value of E_0 that is a factor of 5 smaller. Two points are worth noting from this figure. First, the Δ profile of the LTB void is sensitive to the value of E_0 , although the maximum difference between the two LTB Δ profiles is only at the ~ 10 per cent level. Second, the velocity profile of our void differs substantially from that of the LTB void for either value of E_0 , even though the density profiles of the two voids agree reasonably well (by construction), as shown in Fig. 3.

To determine the CMB temperature decrement produced by our void, we consider an observer comoving with the cosmic fluid in the external universe. The present-day distance of the observer from the void is chosen such that the centre of the void lies at a redshift $z_c = 0.15$. This corresponds to a comoving radial coordinate distance $\hat{r} = 434h^{-1}$ Mpc. Since FGKPS employ the gauge condition $R(\hat{r}, \hat{t}_0) = \hat{r}$ at t_0 , this corresponds simply to a non-comoving radial coordinate distance of $r = 434h^{-1}$ Mpc at the current epoch. The resulting CMB temperature decrement $\Delta T(\theta)$ is plotted in Fig. 5, and is very similar to that obtained by FGKPS, both in terms of its angular profile and central value of $\Delta T \approx -25 \mu\text{K}$. In Fig. 6, we also plot the variation of $\Delta T/T$, as measured by a comoving observer at each point along the path of a photon that passes through the centre of the void,

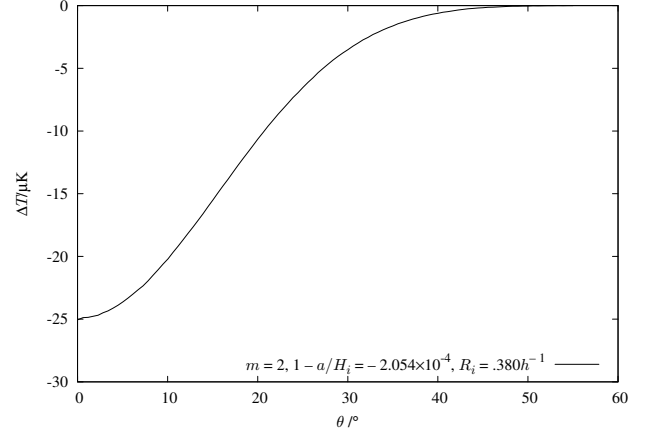


Figure 5. CMB temperature decrement for our void model that best reproduces the present-day density distribution of the FGKPS void. The background CMB temperature is taken to be 2.725K.

which nicely demonstrates that the observer does indeed lie in the external universe, beyond the finite compensation radius of our void.

5.2 Reproducing the velocity profile

Since the velocity profile of our void discussed above differs significantly from that of the FGKPS void, an alternative approach is instead to choose the initial velocity perturbation parameters R_i , a and m such that the resulting present-day velocity profiles of the two voids models are as close as possible. This is achieved by performing an analogous numerical optimisation to that used above.

The resulting present-day density and velocity difference Δ profiles are plotted in Fig. 7, and are compared to those of the FGKPS void model. In this case, one sees that the Δ profiles of the two void models are much closer than what was achieved in the previous subsection, although this comes at the cost of poorer agreement between the density profiles. In particular, the spatial extent of the density profile for our void is larger than in the previous case.

The larger spatial extent of our void model in this case requires us to take care in determining the CMB temperature decrement it produces, since placing the centre of the void at a redshift $z_c = 0.15$ from the observer is insufficient for the observer to reside in the external universe, beyond the finite compensation radius of the void. Nonetheless, this may be achieved by placing the centre of the void at a redshift of $z_c = 0.165$, which corresponds to the observer lying at a radial coordinate distance of $r = 476h^{-1}$ ($= 600$) Mpc. The corresponding CMB temperature decrement is plotted in Fig. 8. As expected, the angular profile of the decrement is larger than that shown in Fig. 5 for our previous void model. Most notable, however, is the central value of $\Delta T \approx -48 \mu\text{K}$, which is almost twice that obtained previously.

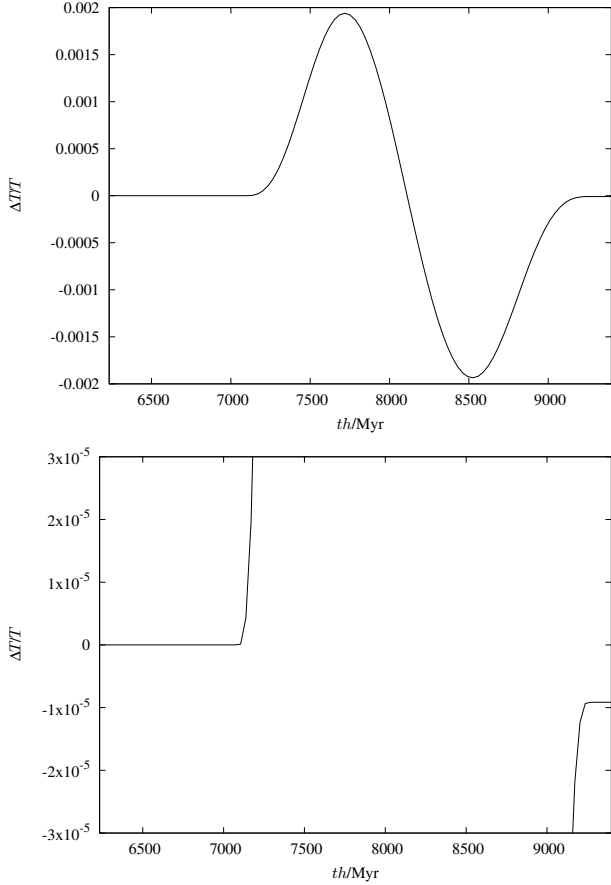


Figure 6. As in Fig. 5, but for the variation of $\Delta T/T$, as measured by a comoving observer at each point along the path of a photon that passes through the centre of the void. The lower panel is identical to the upper panel, but is plotted on an expanded $\Delta T/T$ scale to illustrate the final decrement of $\Delta T/T = -9.16 \times 10^{-6}$.

5.3 Reproducing the density and velocity profiles

The next obvious approach to consider is to choose the initial velocity perturbation parameters R_i , a and m such that the resulting present-day density *and* velocity profiles of our void model match those of the FGKPS void model as closely as possible. As before, this is achieved by performing a numerical optimisation similar to that used above. In this case, however, we employ a chi-squared approach in which the uncertainties on the mismatch are taken to be $\sigma_\delta = 0.01$ and $\sigma_v = 30 \text{ km s}^{-1}$ for the density and velocity profiles, respectively, which ensures that the contribution to the best fit value of χ^2 is roughly similar for the density and velocity profiles. The value of m is fixed to be 2.

The resulting present-day density and velocity difference Δ profiles are plotted in Fig. 9, and are compared to those of the FGKPS void model. As one might expect, both profiles in our void agree reasonably well with those in the FGKPS void, but neither agrees as closely as in the case where the optimisation was performed for that profile alone. In particular, the spatial extent of the density profile is similar to that found when optimising the velocity profile alone, and somewhat larger than when optimising for the density profile alone.

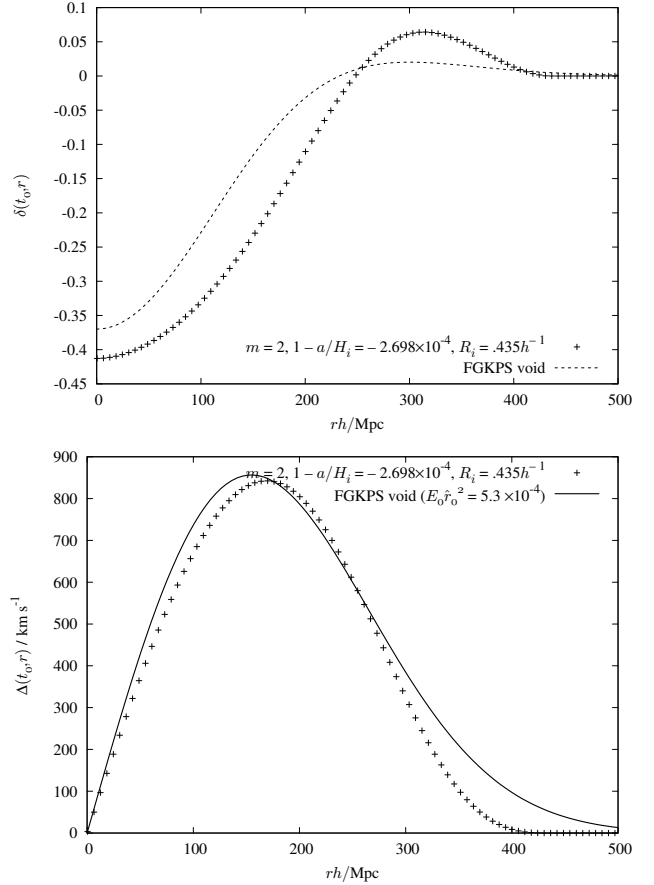


Figure 7. Void density profile (top) and velocity difference Δ profile (bottom) at $t = t_0$ in our model (crosses), resulting from an initial velocity perturbation at $z = 10^3$ with parameters chosen to reproduce the FGKPS void velocity profile (solid line, bottom panel) as closely as possible.

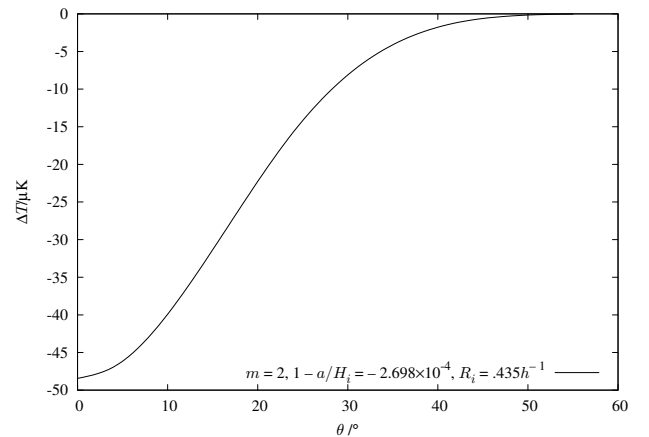


Figure 8. As in Fig. 5, but for our void model that best reproduces the present-day velocity distribution of the FGKPS void.

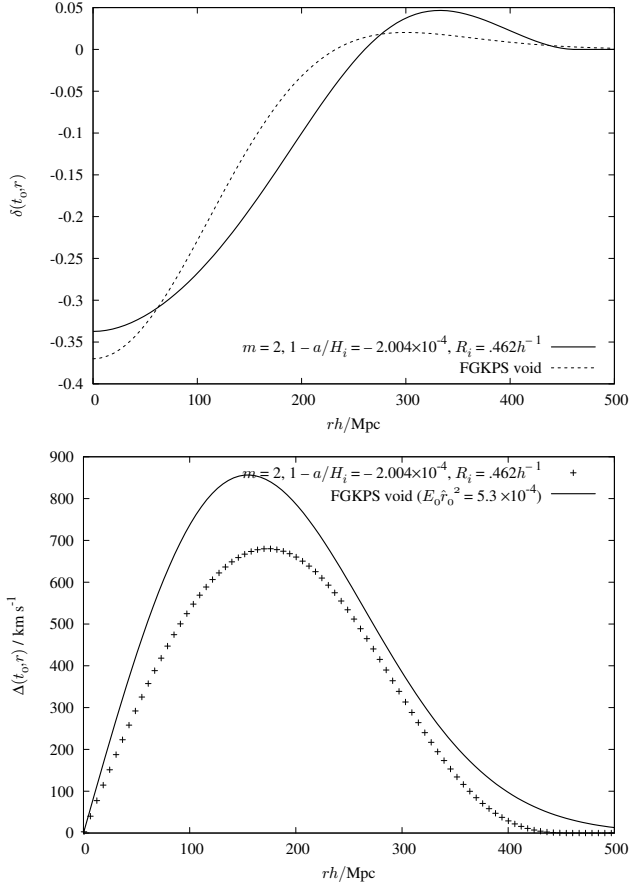


Figure 9. As in Fig. 7, but for an initial velocity perturbation at $z = 10^3$ with parameters chosen to reproduce the FGKPS void density and velocity profile (solid lines) as closely as possible.

As in the previous subsection, the larger spatial extent of our void model requires us to place the centre of the void at a redshift $z_c = 0.165$ from the observer, in order for the observer to be in the external universe. The resulting CMB temperature decrement is shown in Fig. 10, which is similar in both angular extent and depth to that plotted in Fig. 8.

5.4 Consistency with observations

Although we have focussed on comparing the different characteristics of the Draco void models produced by the LTB and tetrad-based approaches, respectively, it is important to determine whether the set of void models produced using our alternative methodology is consistent with observations. In Fig 11, we thus compare the projected density profiles and CMB temperature decrements of our three void models considered in subsections 5.1–5.3 with the WISE-2MASS galaxy catalogue and the Planck CMB data. The data points are taken directly from FGKPS. We see that all three void models are consistent with the WISE-2MASS data. The CMB temperature decrement of our first void model is consistent with the Planck data on all scales, but our second and third void models are consistent with the Planck data only on larger scales, and yield too large a decrement on angular scales below $\sim 20^\circ$.

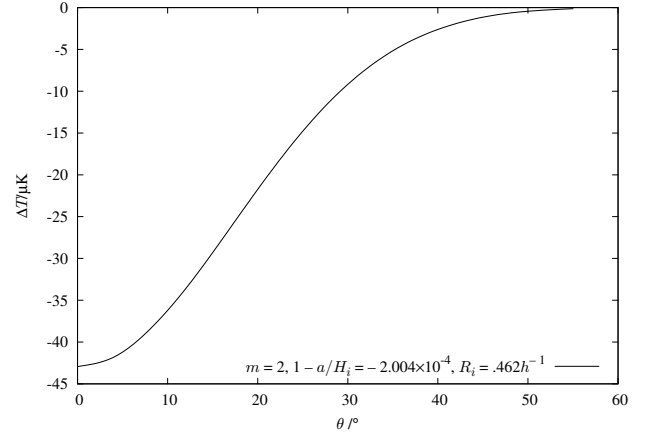


Figure 10. As in Fig. 5, but for our void model that best reproduces the present-day density and velocity distributions of the FGKPS void.

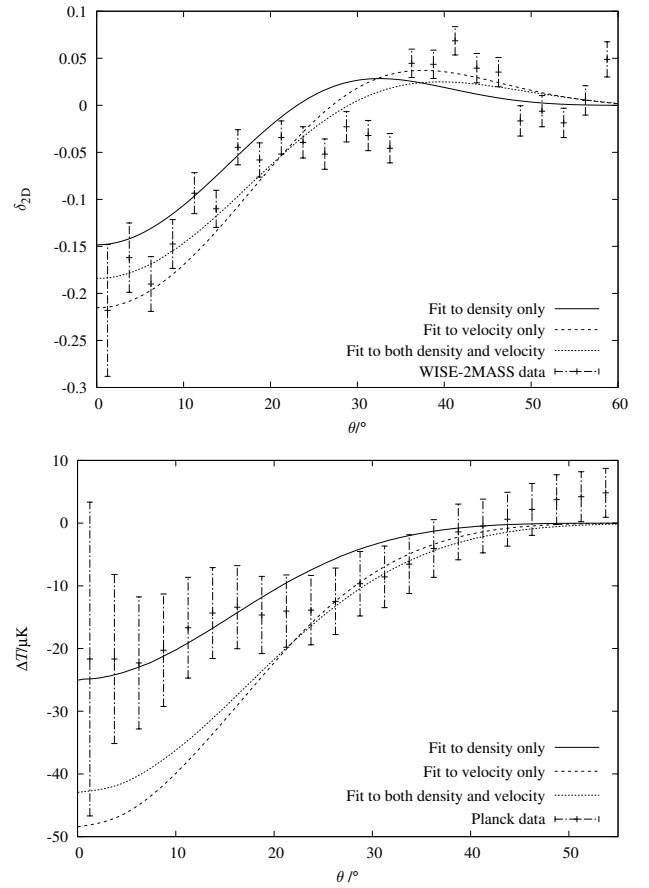


Figure 11. Void projected density profiles (top) and corresponding CMB temperature decrements (bottom) for our three models, compared to data from WISE-2MASS and Planck respectively. Data points are taken from FGKPS.

Although the LTB void model of FGKPS and our three void models are each consistent with the galaxy counts and broadly consistent with CMB observations in the direction of Draco (at least on angular scales $\geq 20^\circ$), it is clear that there remain considerable differences between the models, which result from the different parameterisations that they employ. Indeed, the above investigations show that relatively slight differences in the parameterisation can lead to large changes in the relationship between density and velocity profiles, and very different CMB temperature decrements. Moreover, all of the models considered are consistent with having grown from primordial perturbations in the early universe. One must therefore be careful in drawing conclusions regarding the physical characteristics of voids from data that constrain just their project density distribution and CMB temperature decrement.

6 DE-EVOLVING THE DRACO VOID

In developing the void models investigated thus far, we have been careful to ensure consistency with the void having grown from a primordial perturbation in the early universe. This requirement is, of course, crucial in producing a physically realistic void model. Nonetheless, in this section, we investigate the consequences of neglecting this requirement, with the purpose of demonstrating how tailoring a void to have given characteristics at the present epoch results, in general, in a physically unacceptable model.

To this end, we therefore begin by choosing the parameters R_i , a and m in our velocity perturbation at $z = 10^3$ to produce a velocity profile today that is as close as possible to that of the FGKPS void model. We then choose *different* values, say a_ρ and m_ρ , for these parameters, again at $z = 10^3$, to produce a density profile that mimics that of the FGKPS void as closely as possible. We keep the value of R_i the same in each case, so that the size of the perturbed region is consistent. We also use the same value of H_i , which ensures that the density profile remains compensated.

The resulting density and velocity profiles at the current epoch are shown in Fig. 12. The background Hubble parameter and the spatial extent of the perturbation are taken as $H_i = 70 \text{ km s}^{-1} \text{ Mpc}^{-1}$ and $R_i = 479 h^{-1} \text{ Mpc}$, respectively. The remaining parameter values that best reproduce the FGKPS void density profile are $1 - a_\rho/H_i = -0.0342$ and $m_\rho = 2$, whereas those that best reproduce the FGKPS void velocity profile (bottom) are $1 - a/H_i = -0.0836$ and $m = 2$.

To determine the resulting CMB temperature decrement, the large spatial extent of the void means that one must again place the centre of the void at a redshift larger than $z_c = 0.15$ from the observer for the latter to reside in the external universe. We find that this can be achieved by placing the observer at a radial coordinate distance of $483 h^{-1} \text{ Mpc}$, which corresponds to $z_c \sim 0.167$. The resulting CMB temperature decrement is plotted in Fig. 13. Interestingly, the depth of the decrement is much smaller than found for our previous void models, with a central value of just $\Delta T \approx -9.7 \mu\text{K}$.

One may demonstrate that this void model is physically unrealistic, however, by considering the void with the present-day density and velocity profiles plotted in Fig. 12 and evolving it *backwards* in time. The value of the t param-

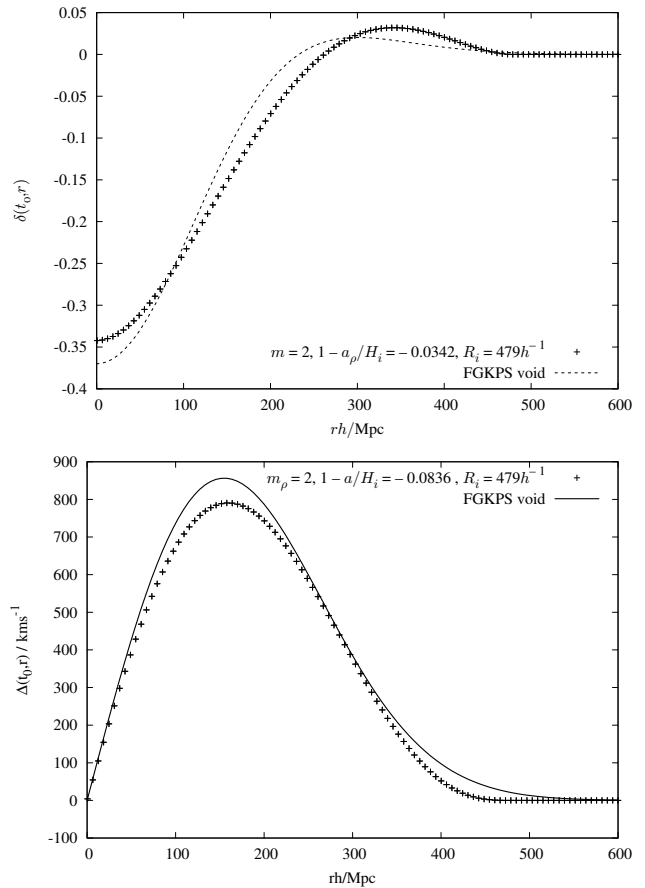


Figure 12. As in Fig. 9, but for two initial velocity perturbations at $z = 10^3$ chosen separately to reproduce the FGKPS void density and velocity profile (solid lines), respectively, as closely as possible, and without requiring the void to be consistent with having grown from a primordial perturbation.

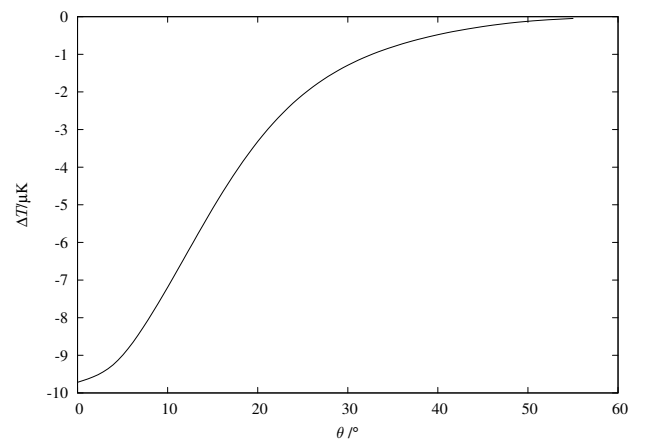


Figure 13. CMB temperature decrement produced by the void with the present-day density and velocity profiles plotted in Fig. 12.

eter corresponding to the current epoch is 13.5 Gyr. The density contrast at a selection of earlier times is shown in Fig. 14. One sees that the density contrast diverges at early epochs. This occurs because the void model contains a decaying mode, which grows as one moves backwards in time. Consequently, this void model is not consistent with having grown from a primordial perturbation. This behaviour is, in fact, quite generic unless one takes care to exclude the decaying mode by choosing the initial density and velocity profiles in the early universe to obey the condition (15).

7 CONCLUSIONS

We apply our tetrad-based approach for constructing spherically-symmetric solutions in general relativity to modelling voids and the secondary anisotropies that they induce in the CMB. We compare our approach to the usual LTB method, and demonstrate that the two methods represent a Eulerian and Lagrangian description, respectively, of the dynamics of a pressureless cosmological fluid.

In particular, we use our approach to construct models for the void observed in the direction of Draco in the WISE-2MASS galaxy survey, and a corresponding CMB temperature decrement in the Planck data in the same direction, and compare our void models with that produced by Finelli et al. (2016) using the LTB formalism. We find that the present-day characteristics of the void, summarised by its current density and velocity profiles, are not well constrained by the existing data, such that a large range of different void models are broadly consistent with the observations. In particular, we note that models derived from different parameterisations of the void typically lead to very different density and/or velocity profiles. CMB temperature decrements are especially sensitive to the velocity profile; however it is often overlooked in LTB models of voids.

Finally, we demonstrate the importance of ensuring that void models are consistent with having evolved from primordial perturbations in the early universe, and hence contain no contribution from a decaying mode. In particular, we show that constructing a void model such that it has given density and velocity profiles at the present epoch will, in general, lead to unphysical singularities in the void model at earlier epochs.

ACKNOWLEDGEMENTS

Do Young Kim is supported by a Samsung Scholarship. We thank Seshadri Nadathur for useful discussions related to over-constraint of an LTB model.

REFERENCES

- Alexander S., Biswas T., Notari A., Vaid D., 2007, *Journal of Cosmology and Astroparticle Physics*, Issue 09, id. 025 (2009)., 9
- Bene G., Csapo A., 2010, preprint ([arXiv:1002.4610](#))
- Bolejko K., C  l  rier M.-N., 2010, *Phys. Rev. D*, 82, 103510
- Bondi H., 1947, *MNRAS*, 107, 410
- Brouzakis N., Tetradis N., Tzavara E., 2006, *Journal of Cosmology and Astroparticle Physics*, Issue 02, id. 013 (2007)., 2
- C  l  rier M.-N., 2012a, preprint ([arXiv:1203.2814](#))
- C  l  rier M.-N., 2012b, *A&A*, 543, A71
- Colless M., et al., 2001, *Monthly Notices of the Royal Astronomical Society*, Volume 328, Issue 4, pp. 1039-1063., 328, 1039
- Dabrowski Y., Hobson M. P., Lasenby A. N., Doran C. J. L., 1998, *MNRAS*, 302, 15
- Dabrowski Y., Hall M. J., Sawicki I. L., Lasenby A. N., 1999, *MNRAS*, 318, 9
- Finelli F., Garcia-Bellido J., Kovacs A., Paci F., Szapudi I., 2014, preprint ([arXiv:1405.1555v1](#))
- Finelli F., Garcia-Bellido J., Kovacs A., Paci F., Szapudi I., 2016, *MNRAS*, 455, 1246
- Garcia-Bellido J., Haugb  lle T., 2008, *J. Cosmol. Astropart. Phys.*, 2008, 003
- Geshnizjani G., Chung D. J. H., Afshordi N., 2005, *Physical Review D*, vol. 72, Issue 2, id. 023517, 72
- Kainulainen K., Marra V., 2009, *Phys. Rev. D*, 80, 127301
- Kim D. Y., Lasenby A. N., Hobson M. P., 2018, *General Relativity and Gravitation*, 50, 29
- Lasenby A., Doran C., Gull S., 1998, *Phil. Trans. R. Soc. Lond. A*, 356, 487
- Lasenby A. N., Doran C. J. L., Hobson M. P., Dabrowski Y., Challinor A. D., 1999, *MNRAS*, 302, 748
- Lavaux G., Wandelt B. D., 2012, *The Astrophysical Journal*, 754, 109
- Lema  tre G., 1933, *Annales de la Soci  t   Scientifique de Bruxelles*, A53, 51
- Mackenzie R., Shanks T., Bremer M. N., Cai Y.-C., Gunawardhana M. L. P., Kov  cs A., Norberg P., Szapudi I., 2017, preprint ([arXiv:1704.03814](#))
- Marcos-Caballero A., Fern  ndez-Cobos   c. R., Mart  nez-Gonz  lez E., Vielva P., 2016, *MNRAS*, 460, 15
- Marra V., Kolb E. W., Matarrese S., Riotto A., 2007a, *Physical Review D*, vol. 76, Issue 12, id. 123004, 76
- Marra V., Kolb E. W., Matarrese S., 2007b, *Physical Review D*, vol. 77, Issue 2, id. 023003, 77
- Nadathur S., Lavinto M., Hotchkiss S., R  s  nen S., 2014, *Phys. Rev. D*, 90, 103510
- Nandra R., Lasenby A. N., Hobson M. P., 2012a, *MNRAS*, 422, 2931
- Nandra R., Lasenby A. N., Hobson M. P., 2012b, *MNRAS*, 422, 2945
- Nandra R., Lasenby A. N., Hobson M. P., 2013, *Phys. Rev. D*, 88, 044041
- Pisani A., Sutter P. M., Hamaus N., Alizadeh E., Biswas R., Wandelt B. D., Hirata C. M., 2015, *Physical Review D - Particles, Fields, Gravitation and Cosmology*, 92
- Romano A. E., Vallejo S. A., 2015, *EPL*, 109, 39002
- Siegel E. R., Fry J. N., 2005, *The Astrophysical Journal*, Volume 628, Issue 1, pp. L1-L4., 628, L1
- Sutter P. M., Lavaux G., Wandelt B. D., Weinberg D. H., 2012, *The Astrophysical Journal*, 761, 44
- Tegmark M., et al., 2003, *The Astrophysical Journal*, Volume 606, Issue 2, pp. 702-740., 606, 702
- Tokutake M., Yoo C.-M., 2016, preprint, p. 12 ([arXiv:1603.07837](#))
- Tolman R. C., 1934, *Proc. Natl. Acad. Sci. U.S.A.*, 20, 169
- Zibin J. P., 2008, *Physical Review D*, 78, 043504
- Zibin J., 2014, preprint ([arXiv:1408.4442](#))
- Zibin J. P., Moss A., Scott D., 2008, *Physical Review Letters*, 101, 251303

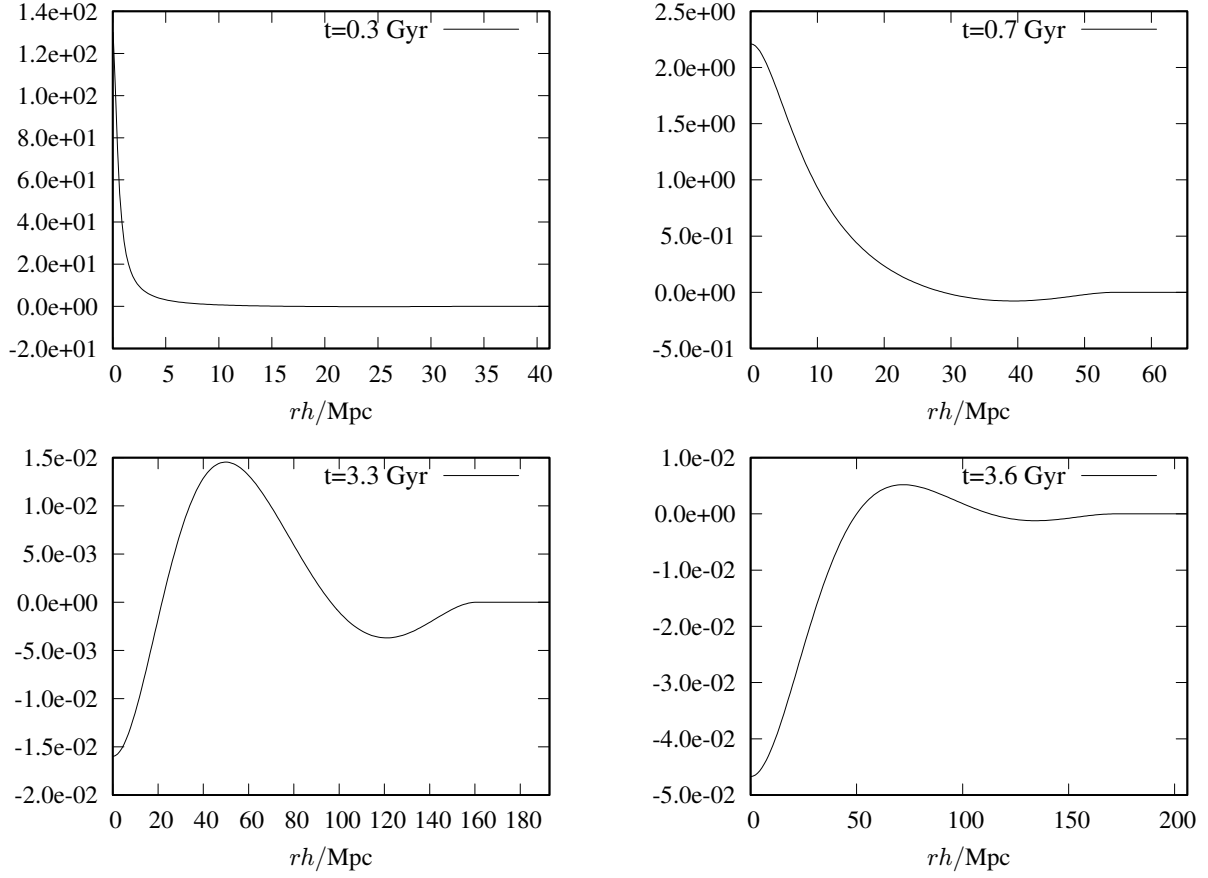


Figure 14. The density contrast at a selection of earlier epochs for the void with the present-day ($t = 13.5 \text{ Gyr}$) density and velocity profiles plotted in Fig. 12.